Eur J Nucl Med Mol Imaging (2017) 44:1721–1731
DOI 10.1007/s00259-017-3697-1

ORIGINAL ARTICLE

[18]Fluorodeoxyglucose Positron Emission Tomography for the Textural Features of Cervical Cancer Associated with Lymph Node Metastasis and Histological Type

Wei-Chih Shen[1] · Shang-Wen Chen[2,3,4,5] · Ji-An Liang[2,5] · Te-Chun Hsieh[6,7] · Kuo-Yang Yen[6,7] · Chia-Hung Kao[5,6,8]

Received: 7 December 2016 / Accepted: 28 March 2017 / Published online: 14 April 2017

Abstract

Background In this study, we investigated the correlation between the lymph node (LN) status or histological types and textural features of cervical cancers on ^{18}F-fluorodeoxyglucose positron emission tomography/computed tomography.

Methods We retrospectively reviewed the imaging records of 170 patients with International Federation of Gynecology and Obstetrics stage IB–IVA cervical cancer. Four groups of textural features were studied in addition to the maximum standardized uptake value (SUV_{max}), metabolic tumor volume, and total lesion glycolysis (TLG). Moreover, we studied the associations between the indices and clinical parameters, including the LN status, clinical stage, and histology. Receiver operating characteristic curves were constructed to evaluate the optimal predictive performance among the various textural indices. Quantitative differences were determined using the Mann–Whitney U test. Multivariate logistic regression analysis was performed to determine the independent factors, among all the variables, for predicting LN metastasis.

Results Among all the significant indices related to pelvic LN metastasis, homogeneity derived from the gray-level co-occurrence matrix (GLCM) was the sole independent predictor. By combining SUV_{max}, the risk of pelvic LN metastasis can be scored accordingly. The TLG_{mean} was the independent feature of positive para-aortic LNs. Quantitative differences between squamous and nonsquamous histology can be determined using short-zone emphasis (SZE) from the gray-level size zone matrix (GLSZM).

Conclusion This study revealed that in patients with cervical cancer, pelvic or para-aortic LN metastases can be predicted by using textural feature of homogeneity from the GLCM and $TLG_{mean,}$ respectively. SZE from the GLSZM is the sole feature associated with quantitative differences between squamous and nonsquamous histology.

Shang-Wen Chen and Wei-Chih Shen are equally contributory to this article.

Electronic supplementary material The online version of this article (doi:10.1007/s00259-017-3697-1) contains supplementary material, which is available to authorized users.

✉ Chia-Hung Kao
d10040@mail.cmuh.org.tw

[1] Department of Computer Science and Information Engineering, Asia University, Taichung, Taiwan

[2] Department of Radiation Oncology, China Medical University Hospital, Taichung, Taiwan

[3] School of Medicine, China Medical University, Taichung, Taiwan

[4] School of Medicine, Taipei Medical University, Taipei, Taiwan

[5] Graduate Institute of Clinical Medical Science, School of Medicine, College of Medicine, China Medical University, No. 2, Yuh-Der Road, Taichung 40447, Taiwan, Republic of China

[6] Department of Nuclear Medicine and PET Center, China Medical University Hospital, Taichung, Taiwan

[7] Department of Biomedical Imaging and Radiological Science, China Medical University, Taichung, Taiwan

[8] Department of Bioinformatics and Medical Engineering, Asia University, Taichung, Taiwan

Keywords Cervical cancer · ^{18}F-fluorodeoxyglucose positron emission tomography · Intratumor heterogeneity · Texture analysis · Lymph node status

Abbreviations

PET/CT	Positron emission tomography/computed tomography
SUV_{max}	maximum standardized uptake value
TLG	total lesion glycolysis
MTV	metastatic tumor volume
SZE	short-zone emphasis

Introduction

Intratumoral heterogeneity plays a crucial role in the proliferation, vascular supply, and metabolism of various solid malignancies [1]. Such biological characteristics are vital because they are often associated with aggressiveness or sensitivity to a specific therapy. Currently, ^{18}F-fluorodeoxyglucose (FDG) positron emission tomography/computed tomography (PET/CT) is widely used for staging and monitoring various cancers. The uptake heterogeneity observed within tumors assayed through FDG PET is increasingly believed to be of prognostic value [2, 3]. In addition, the measurement of textural indices from tumor PET images has recently been proposed as an adjunct to predict tumor responses to a therapy [4–13]. Compared with the maximum standard uptake value (SUV_{max}), metabolic tumor volume (MTV), and total lesion glycolysis (TLG) alone, the uptake distribution within a tumor can theoretically provide more insight into the underlying tumor biology. On the basis of this assumption, researchers have studied ^{18}F-FDG uptake heterogeneity in various tumors by computing textural indices in baseline PET images.

Clinical stage and lymph node (LN) metastasis are major determinants of both disease-free and overall survival in patients with cervical carcinoma [14, 15]. Studies have indicated that the uptake heterogeneity observed within tumors on FDG PET may be of prognostic value [9–11]; however, to date, few studies have reported an association between intratumoral FDG uptake heterogeneity and clinical parameters in this cancer setting. Theoretically, textural features associated with adverse clinical parameters may play a role in treatment outcomes. We hypothesized that textural features derived from the FDG uptake heterogeneity of cervical tumors may correlate with LN involvement, clinical stage, and histological types. Particularly, despite PET/CT having a high sensitivity and specificity for detecting LN metastasis [15–17], such an association has not been reported. To provide a new avenue for studying the underlying mechanisms of textural features, more information is required on the association of underlying biological characteristics and clinical parameters with comprehensive textural features.

Materials and Methods

Study population

In this retrospective cohort study, we enrolled 170 patients (median age, 55 years) newly diagnosed as having cervical cancer at China Medical University Hospital between July 2009 and December 2015. All the patients had undergone pretreatment (^{18}F-FDG PET/CT) for radiotherapy planning or pretreatment staging. Patients with a history of diabetes were excluded, and all the patients had normal serum glucose levels before undergoing PET/CT. The minimum size of the eligible criteria for the primary tumors was maximal diameter ≥2 cm in computed tomogram. Only primary tumors were considered because a reliable textural analysis of small lesions is difficult owing to the small number of voxels involved. This study was approved by a local institutional review board [DMR99-IRB-010(CR6)]. We performed tumor staging according to the International Federation of Gynecology and Obstetrics (FIGO) and observed that 41, 91, 35, and 3 patients had stage I, II, III, and IVA cancers, respectively. PET/CT has a high sensitivity and specificity for detecting the nodal status in cervical cancer [15–17]; therefore, it was performed for diagnosing pelvic LNs (PLNs) or para-aortic LN (PALN) metastasis [16]. Briefly, experienced nuclear medicine physicians performed a visual analysis by using a five-point scoring system (0, normal; 1, probably normal; 2, equivocal; 3, probably abnormal; and 4, definitely abnormal), which had been routinely used in interpreting FDG PET/CT images in our institution. We used dichotomous variables in this study: a score 3 or 4 was considered to have LN metastasis, and score 0, 1, or 2 was regarded as absence of metastasis. Accordingly, we identified ≥1 PLNs and ≥1 PALNs in 84 and 25 patients, respectively. Table 1 lists the patient characteristics.

Training and validation cohorts

Because the large number of patients had PLN metastasis, we divided the 170 patients into two cohorts (85 for training, 85 for validation) to confirm the reliability of predictors for PLN metastasis. The first cohort came from patient lists between July 2009 and June 2013, whereas the validation cohort consisted of patients with pretreatment PET/CT after June 2013. Basically, the two cohorts received the same protocol of PET/CT imaging and interpretation which would be mentioned below. The presence of ≥1 PLN metastasis was identified in 44 and 40 patients for the training and validation cohorts, respectively.

Table 1. Patient characteristics (n = 170)

Variables	Value
Age (year)	Median 55 (range, 24 ~ 85)
FIGO stage	
IB	41 (24%)
IIA–IIB	91 (53%)
IIIA–IIIB	35 (21%)
IVA	3 (2%)
Histology	
Squamous cell carcinoma	138 (81%)
Adenocarcinoma	30 (18%)
Adenosqumous cell carcinoma	2 (1%)
Maximal tumor diameter	
<4 cm	36 (21%)
<6 cm and ≧4cm	102 (60%)
≧6 cm	32 (19%)
Pelvic LN metastasis	
Negative	86 (51%)
Positive	84 (49%)
Paraaortic LN metastasis	
Negative	145 (85%)
Positive	25 (15%)
SUVmax	Mean 11.3 ± 5.8 (range, 2.9 ~ 37.0)
MTV(ml)	Mean 33.3 ± 35.6 (range, 2.5 ~ 450.0)
TLG mean (g)	Mean 248.2 ± 264.8 (range, 4.7 ~ 1800.9)
Treatment	
Chemoradiotherapy	150 (88%)
Radiotherapy alone	20 (12%)

Abbreviations: FIGO = International Federation of Gynecology and Obstetrics; MTV = volume using fixed thresholds of 50% of the SUV_{max}; TLG_{mean} = the SUV_{mean} multiplied by the volume by using fixed thresholds of 50% of the SUV_{max}.

Note: The maximal tumor diameter was measured according to horizontal length of tumor on axial view of pretreatment CT scan.

On the other hand, owing to the limited number of patients with PALN metastasis or nonsquamous histology, the split of the patients into two cohorts was not employed in the same way when analyzing PALN metastasis or histological types.

PET/CT imaging

All patients were scanned using a PET/CT scanner (PET/CT: 16 slices; Discovery STE; GE Medical System, Milwaukee, WI, USA). The patients were requested to fast for at least 4 hours before undergoing FDG PET/CT, and the technique was conducted approximately 60 min after the administration of 370 MBq of ^{18}F-FDG. Thus, FDG uptake was determined by calculating the SUV. The procedure was previously described [18].

Delineation of the metabolic tumor volume of cervical tumors

The MTV of a cervical tumor was delineated by using the region growing and excluding the bladder if it was connected. In the PET volume, the voxel was defined as a local maximum if its SUV was not less than those of all neighbors. The SUV_{max} identified by the user indicated the largest uptake among all local maxima within a cervical tumor, and was used as the initial seed point for a region growing procedure. The region growing procedure delineates the MTV as all voxels connected to SUV_{max} that have an SUV not less than a specified fraction of SUV_{max}. The threshold used in this study was 50% of SUV_{max}. Although it is debatable to limit the inclusion of nonpathological adjacent organs in the heterogeneity analysis, the decision of the spatial extent of a MTV delineated by a fixed threshold at 50% of SUV_{max} was a trade-off between the adequate separation and the sufficient intratumoral uptakes. If the bladder was not included, the formed region was defined as the MTV of the cervical tumor. Otherwise, the SUV_{max} of the bladder was identified and created a new region by using the same aforementioned criteria. The new region was partitioned into several spherical objects by employing watershed transform technique [19]. The objects belonging to the bladder were manually identified and excluded from the region, whereas the remaining areas were integrated and defined as the MTV of the cervical tumor. The TLG_{mean} was calculated by multiplying the SUV_{mean} of the cervical tumor by the MTV.

Calculation of textural indices

Discretization of the SUVs within the previously delineated MTV was the fundamental for the calculation of textural indices. Two types of the discretization method were employed to divide the SUV range within the MTV into a fixed number of bins or into a fixed bin size. The discretization method using a fixed number of bins divided the SUV range into 4, 8, 16, 32, 48, 64, 80, 96, 112, or 128 bins, respectively. The SUV range was resampled by a width of 0.01, 0.025, 0.05, 0.075, 0.1, 0.25, 0.5, 0.75, or 1 g/ml when the discretization method using a fixed bin size. For all quantization results acquired from each parameter of a discretization method, we calculated four matrices to evaluate the heterogeneity, namely the gray-level co-occurrence matrix (GLCM) [20], neighboring gray-level dependence matrix (NGLDM) [21], gray-level run length matrix (GLRLM) [22], and gray-level size zone matrix (GLSZM) [23]. That is, a total of 76 matrices (10*4 + 9*4) were calculated. Moreover, 18-connectivity is used to describe the relationship between any two adjacent voxels. In the GLCM and GLRLM, the neighbor of each voxel (x, y, and z) within a cervical tumor is defined to be the located within the offset (0, 1, and 0). For every parameter of a discretization

method, a total of 33 texture indices listed in Appendix 1 were derived from the four matrices [20–23].

Statistical analysis

In this study, PET/CT was performed to correlate various textural indices with clinical parameters to determine the optimal indices for predicting LN metastasis and differentiating clinical stages and histological types. Receiver operating characteristic (ROC) curves were constructed to evaluate the optimal predictive performance among the SUV_{max}, MTV, and TLGs, and four groups of textural indices. In addition, serum tumor markers, namely squamous cell carcinoma antigen (SCC-Ag) and carcinoembryonic antigen (CEA), were analyzed. Quantitative differences in all variables between LN groups and histological types were determined using the Mann–Whitney U test. Kruskal–Wallis and post-hoc tests were used to examine the correlation between tumor stages and textural indices. In addition, we used multivariate logistic regression analysis to determine the independent factors among all the variables for predicting LN metastasis. Two-tailed tests were used, and $P < 0.05$ was considered statistically significant. All calculations were performed using SPSS 13.0 for Windows (SPSS Inc., Chicago, IL, USA).

Results

Selection of the discretization method and parameter setting

The selection of the discretization method and its parameter setting was determined by the performance of the indices in predicting PLN metastasis. In the process of the discretization, the SUV range within the MTV was quantized by a specific parameter and then used to derive textural features. Then, the advantage of a discretization method was evaluated by the performances of the derived textural indices by the ROC curves in terms of PLN metastasis. For the textural indices obtained from all parameters per discretization method, all acquired areas were averaged as listed in Appendix 1. In this study, the area under the ROC curve was regarded as significant if the value was greater than 0.7 or less than 0.3. There were 4, 4, 5, and 2 textural indices with significant performance when a fixed number of bins was used in the discretization method. In contrast, 3, 1, 1, and 1 indices were significant if a fixed bin size was adopted in the discretization method. Obviously, the indices derived from the discretization method using a fixed number of bins demonstrated a better performance than those using a fixed bin size. Moreover, the areas of the ROC curves originated from the discretization method using four bins were generally greater than those using the other number of bins. As a result, all textural indices presented in this study were derived from the same quantized results of the discretization method.

Predictive value of textural indices for PLN metastasis

We retrieved the four groups of textural indices and various thresholds of classical MTVs and TLGs. As summarized in Table 2, the ROC curves indicated that among several indices in the four groups of textural features, conventional PET/CT parameters and serum SCC-Ag levels were predictors of PLN metastasis in both cohorts. Numerous indices across the groups were positively associated with PLN metastasis, whereas some showed a negative correlation. All the statistically significant indices were subjected to multivariate logistic regression analysis. In the training cohort, the homogeneity index derived from the GLCM [$P < 0.00001$, odds ratio (OR) = 648938.3, 95% confidence interval (CI) = 634.7–6635245.2] was the sole independent predictor of PLN metastasis. As listed in Table 2, the predictive parameters identified through ROC curves and logistic regression analysis in the training cohort were tested in the validation cohort. The results revealed that the homogeneity index from the GLCM ($P = 0.001$, OR = 636572.4, 95% CI = 178.3–2.27E+009) remained the single predictor of PLN metastasis, whereas increased SUV_{max} showed a marginal impact ($P = 0.05$, OR = 1.09, 95% CI = 0.999–1.19) in the validation cohort. Although the SUV_{max} did not serve as a consistent predictor between the cohorts, this parameter was an independent factor of PLN metastasis when lumping the whole data together ($P = 0.01$, OR = 1.08, 95% CI = 1.02–1.15). Figure 1 presents the quantitative differences in the SUV_{max} and homogeneity values between the PLN-positive and PLN-negative groups. The mean SUV_{max} for PLN-positive and PLN-negative patients was 12.3 ± 5.7 and 10.4 ± 5.8, respectively, whereas the mean homogeneity values for the two groups were 0.64 ± 0.08 and 0.57 ± 0.07, respectively. Figure 2 shows the scatterplot between these groups. The homogeneity index seems to be a more accurate predictor of PLN metastasis than does the SUV_{max}.

Risk stratification of PLN metastasis according to adverse imaging features

Because the use of SUV_{max} has become a standard component of diagnosis and staging in oncology, we postulated a risk stratification of PLN metastasis according to the median values of SUV_{max} and homogeneity index. The patients were classified into three risk groups. Group A comprised 43 patients with less than 50% of both SUV_{max} and homogeneity (median SUV_{max} and homogeneity: 10.4 and 0.61, respectively). Group B comprised 84 patients with one of the 2 factors,

Table 2. Predictive textural indices for pelvic lymph node metastasis and the area under the ROC curve in training and validation cohorts

Classification of matrix	Index	AUC Training/validation	*P* value Training/validation
Tumor marker	SCC-Ag	0.65 ± 0.06/0.67± 0.06	0.02/0.01
	CEA	0.59 ± 0.06/0.48± 0.07	0.15/0.70
Conventional PET-related parameter	SUV_{max}	0.61 ± 0.06/0.64± 0.06	0.09/0.03
	MTV	0.76 ± 0.05/0.72± 0.06	<0.001/0.001
	TLG_{mean}	0.77 ± 0.05/0.75± 0.05	<0.001/<0.001
Gray-level cooccurrence matrix (GLCM)	Contrast	0.22 ± 0.05/0.28± 0.06	<0.001/0.001
	Correlation	0.75 ± 0.05/0.70± 0.006	<0.001/0.02
	Dissimilarity	0.22 ± 0.05/0.27± 0.06	<0.001/<0.001
	Energy	0.71 ± 0.06/0.59± 0.06	0.001/0.14
	Entropy	0.31 ± 0.06/0.42± 0.06	0.002/0.19
	Homogeneity	0.78 ± 0.05/0.73± 0.05	<0.001/<0.001
Gray-level run length matrix (GLRLM)	SRE	0.26 ± 0.05/0.33± 0.06	<0.001/0.005
	LRE	0.78 ± 0.05/0.73± 0.06	<0.001/<0.001
	GLNUr	0.76 ± 0.05/0.70± 0.06	<0.001/0.001
	RP	0.70 ± 0.06/0.68± 0.06	0.001/0.005
	RLNU	0.70 ± 0.06/0.69± 0.06	0.002/0.003
	HGRE	0.33 ± 0.06/0.44± 0.06	0.006/0.31
	SRLGE	0.36 ± 0.06/0.37± 0.06	0.03/0.03
	SRHGE	0.27 ± 0.06/0.41± 0.06	<0.001/0.16
	LRLGE	0.78 ± 0.05/0.69± 0.06	<0.001/0.003
	LRHGE	0.68 ± 0.06/0.63± 0.06	0.005/0.03
Neighborhood gray-level different matrix (NGLDM)	Coarseness	0.26 ± 0.05/0.29± 0.06	<0.001/0.001
	Contrast	0.22 ± 0.05/0.28± 0.06	<0.001/0.001
	Busyness	0.76 ± 0.05/0.70± 0.006	<0.001/0.001
	Complexity	0.23 ± 0.05/0.28± 0.06	<0.001/<0.001
	Strength	0.29 ± 0.06/0.29± 0.06	0.001/0.001
Gray-level zone length matrix (GLSZM)	LZE	0.78 ± 0.05/0.73± 0.05	<0.001/<0.001
	ZP	0.23 ± 0.05/0.28± 0.06	<0.001/0.001
	HGZE	0.58 ± 0.06/0.62± 0.06	0.21/0.06
	LZLGE	0.79 ± 0.05/0.72± 0.06	<0.001/0.001
	LZHGE	0.76 ± 0.05/0.73± 0.06	<0.001/0.001

Abbreviations: SCC-Ag = squamous cell carcinoma antigen; CEA = carcinoembryonic antigen; SRE = short-run emphasis; LRE = long-run emphasis; LGRE = low gray-level run emphasis; HGRE = high gray-level run emphasis; GLNUr = gray-level nonuniformity for run; RLNU = run-length nonuniformity; RP = run percentage; HGRE = high gray-level run emphasis; SZLGE = short-zone low gray-level emphasis; SZHGE = short-zone high gray-level emphasis; SRLGE = short-run low gray-level emphasis; SRHGE = short-run high gray-level emphasis; LRLGE = long-run low gray-level emphasis; LRHGE = long-run high gray-level emphasis; LZE = long-zone emphasis; ZP = zone percentage ; HGZE = high gray-level zone emphasis; LZLGE = long-zone low gray-level emphasis; LZHGE = long-zone high gray-level emphasis.

and group C included 43 patients with ≥50% of both risk factors. Accordingly, the estimated risk of PLN metastasis was 23%, 50%, 74% in groups A, B, and C, respectively.

Predictive value of textural indices for PALN metastasis

Table 3 shows that several textural features among the four groups, MTV, TLG, and serum SCC-Ag levels were related to PALN metastasis. Multivariate logistic regression analysis revealed the TLG_{mean} (P = 0.001, OR = 1.004, 95% CI = 1.001–1.006) as the sole independent feature of PALN metastasis. Figure 3 shows the quantitative differences in the TLG_{mean} values between the PALN-positive and PALN-negative groups. The TLG_{mean} for PALN-positive and PALN-negative patients was 531.1 ± 12.8 and 199.4 ± 4.7, respectively. The risk of PALN in patients with <50 and ≥50 percentile of TLG values was 6% and 24%, respectively.

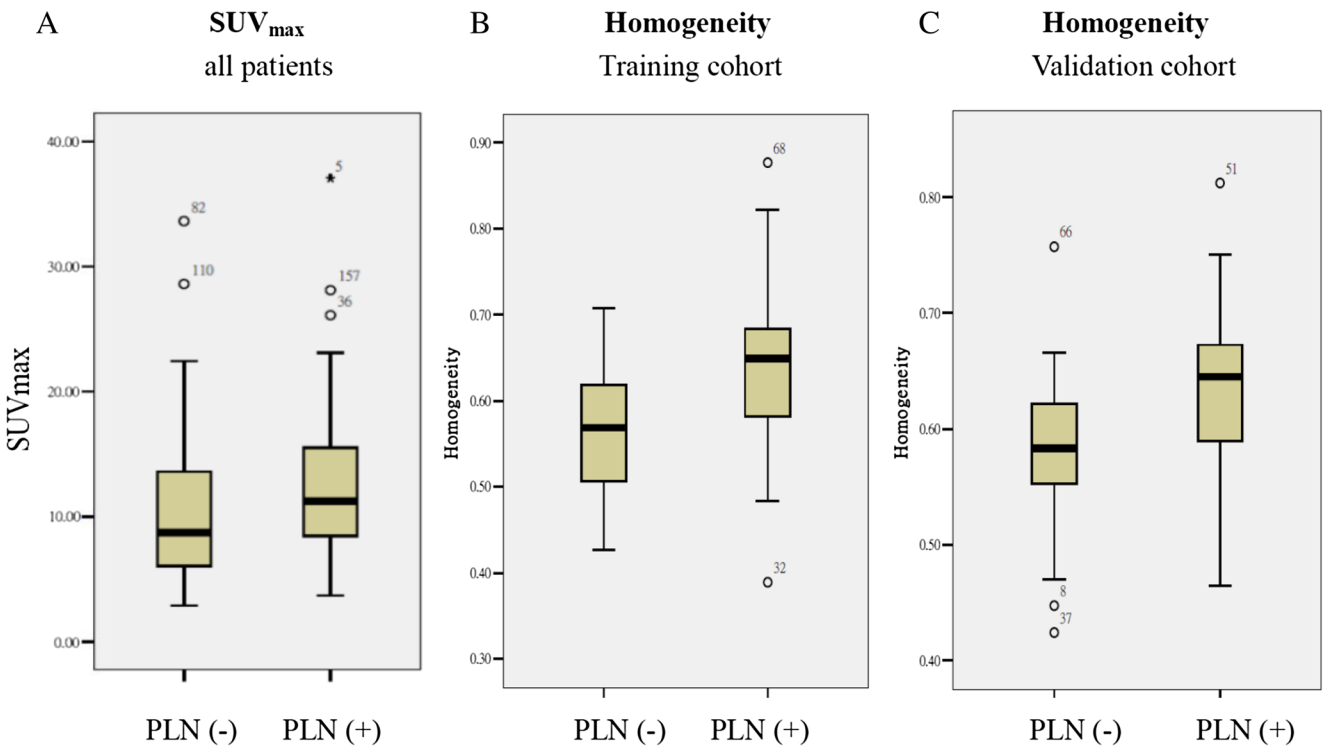

Fig. 1 Quantitative differences in the SUV_{max} values in all patients (1A), homogeneity in training cohort (1B), and homogeneity in validation cohort (1C) of the primary tumors between the pelvic lymph node (PLN)-positive and PLN-negative patients.

Correlation of textural indices with FIGO stage

When the patients were classified into three groups according to the FIGO stage (I, II, and III–IVA), serum SCC-Ag, conventional PET-related parameters, and numerous indices revealed the differences between stage I and III–IVA as well as between stage II and III–IVA (Table 4). However, the imaging variables did not differ significantly between stages I and II. On dichotomizing the patients into stage I, II, and III–IVA, most indices showed a diverging trend (Appendix 2).

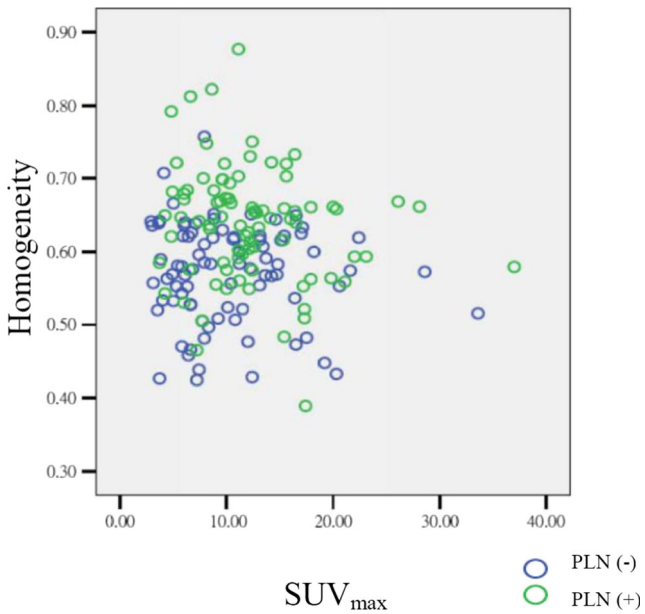

Fig. 2 Scatterplot of the SUV_{max} and homogeneity of the primary tumors according to pelvic lymph node (PLN) metastasis status.

Association of textural indices for histological types

The tumor histology was dichotomized into squamous cell carcinoma (SCC; n = 138) and nonsquamous cell carcinoma (NSCC; n = 32). NSCCs are a histological type of adenocarcinoma or adenosquamous carcinoma. The extracted MTV did not significantly vary between the two groups. The MTV_{mean} was 31.9 ± 32.2 and 39.8 ± 51.6 mL for the SCC and NSCC groups, respectively (P = 0.67 using a Mann–Whitney U test). As summarized in Table 5, short-zone emphasis (SZE) derived from the GLSZM was the sole textural index associated with quantitative differences between the two groups. The mean SZE for SCC and NSCC was 0.30 ± 0.15 and 0.38 ± 0.15, respectively (Fig. 4).

Discussion

An advanced FIGO stage and LN metastases have prognostic value in cervical cancer; however, the association between these clinical parameters and intratumoral FDG PET uptake or underlying textural features remains unclear. In this study, textural indices were used to provide a novel insight on the effects of FDG uptake heterogeneity on the outcomes in some patients

Table 3. Predictive textural indices for para-aortic lymph node metastasis and the area under the ROC curve in whole patients (n = 170).

Classification of matrix	Index	AUC	*P* value
Tumor marker	SCC-Ag	0.65 ± 0.06	0.017
	CEA	0.58 ± 0.07	0.218
Conventional PET-related parameter	SUV_{max}	0.57 ± 0.06	0.274
	MTV	0.74 ± 0.06	<0.001
	TLG_{mean}	0.74 ± 0.05	<0.001
Gray-level cooccurrence matrix (GLCM)	Correlation	0.68 ± 0.06	0.004
	Dissimilarity	0.31 ± 0.06	0.003
	Homogeneity	0.69 ± 0.06	0.002
	Entropy	0.38 ± 0.06	0.047
Gray-level run length matrix (GLRLM)	SRE	0.33 ± 0.06	0.006
	LRE	0.71 ± 0.06	0.001
	GLNUr	0.74 ± 0.06	<0.001
	RP	0.73 ± 0.06	<0.001
	RLNU	0.73 ± 0.05	<0.001
	SRLGE	0.36 ± 0.06	0.029
	LRLGE	0.66 ± 0.06	0.009
	LRHGE	0.65 ± 0.06	0.018
Neighborhood gray-level different matrix (NGLDM)	Coarseness	0.25 ± 0.05	<0.001
	Contrast	0.28 ± 0.06	<0.001
	Busyness	0.74 ± 0.06	<0.001
	Complexity	0.27 ± 0.06	<0.001
	Strength	0.26 ± 0.06	<0.001
Gray-level zone length matrix (GLSZM)	LZE	0.72 ± 0.06	0.001
	GLNUz	0.66 ± 0.06	0.011
	ZP	0.31 ± 0.06	0.003
	LZLGE	0.71 ± 0.05	0.001
	LZHGE	0.72 ± 0.06	<0.001

Abbreviations are the same as those for Table 2.

with cancer who exhibit nodal involvement or advanced stage. In addition, our study is the first to indicate that SZE from the GLSZM are associated with tumors of NSCC. Furthermore, we observed that advanced-stage tumors are associated with quantitative differences in several textural features. Although our findings must be validated, the novel discovery of this study can be applied to and tested for other cancers.

In this study, comprehensive matrix indices [13] were defined to minimize disparities among studies and avoid neglecting useful indices. In addition, bin number and interval setting were varied to quantize the SUVs within the MTV of cervical tumors. Subsequently, the texture indices were calculated under different quantization methods and parameters. The final selection of the quantization method and parameter is determined by the performance in differentiating LN metastasis. Although we found that the best predictive values could be achieved when the SUVs within the MTV of a cervical tumor were quantized into four bins, an additional approach is required to clarify the effects of the different setting of quantization methods and parameters to maximize the clinical importance of texture analysis.

Textural quantification may provide valuable complementary information compared with directly visualizing the retroperitoneal LN through FDG PET alone. Theoretically, a combination of textural parameters can be assumed have a higher correlation with a specific underlying physiological process compared to a single feature [4]. On the basis of our study, with a combination of SUV_{max} and homogeneity index, the pelvic lymphatics of patients with high-risk features, such as group B and C patients, should be more aggressively treated. For example, the irradiation field or dose can be adjusted or optimized.

In a retrospective study conducted by Brooks et al. [24], FDG PET images of 47 PLN-negative and 38 PLN-positive patients with FIGO stage IIb SCCs were analyzed. They observed no statistically significant differences between the two groups for any metric or plausible combination and explained the results with two main reasons. First, the precise uptake heterogeneity observed in other tumor types may not be applicable to cervical carcinomas. Second, the patient population lacked variation. Consequently, the apparent FDG uptake heterogeneity is probably a statistical effect of the partial volume attenuation of markedly different tumor types, shapes, and sizes.

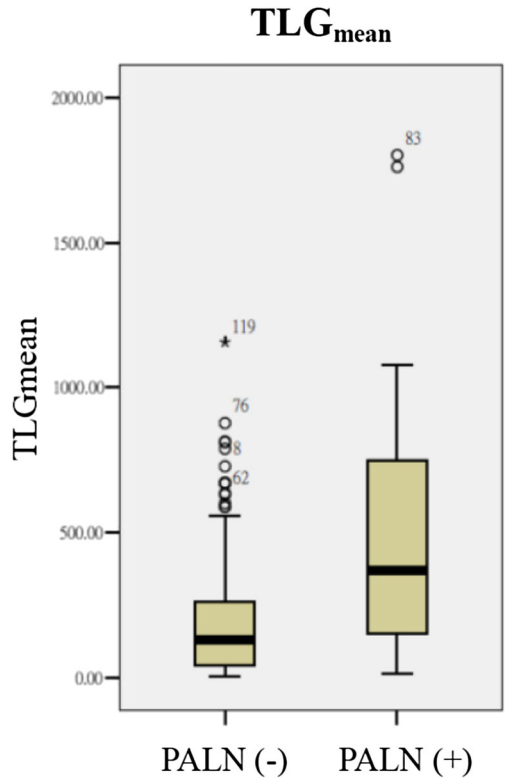

Fig. 3 Quantitative differences in the TLG_{mean} values of the primary tumors between the para-aortic lymph node (PALN)-positive and PALN-negative patients.

The clinical feasibility of textural indices depends on their repeatability and reproducibility. The major determinants included the delineation of the MTV [25], reconstruction protocols of PET images [25], discretization methods [26–28], and PET images acquired at different times [29, 30]. In this study, the MTV delineation and the discretization methods played a major role. If the separation of the MTVs between the cervical tumor and the connected bladder was conducted manually by the user, the acquired MTV might be susceptible to a lack of reproducibility. Therefore, it is imperative to develop an automatic and standardized separation method to minimize this limitation. Besides, the selection of discretization method would affect the quantization results and transform the performance of the textures [26–28]. Because this study aimed to find the ability of textural indices in predicting PLN metastasis, we compared the performance of the two discretization methods to circumvent the limitation. In addition, the standard deviation for the areas under the ROC curves could be used to assess the reproducibility. For example, the standard deviation of the homogeneity in predicting PLN metastasis was 0.017. The low values might imply a high reproducibility of the index.

In this study, when the SUVs of the MTV were quantized into 4, 8, 16, 32, 48, 64, 80, 96, 112, and 128 bins, the areas under the ROC curves for the homogeneity in detecting PLN metastasis were 0.751, 0.747, 0.739, 0.725, 0.721, 0.714, 0.722, 0.715, 0.704, and 0.703, respectively, which evidenced

Table 4. Kruskal–Wallis and Mann–Whitney tests comparing the association between FIGO stages and textural features

Classification of Matrix	Index	Overall difference	Difference between groups		
			Stage I vs. stage II	Stage I vs. stage III-IVA	Stage II vs. stage III–IVA
Tumor marker	SCC-Ag	<0.001		0.002	<0.001
	CEA	0.05		0.022	
Conventional PET-related parameter	SUV_{max}	0.018		0.004	
	MTV	<0.001		<0.001	<0.001
	TLG_{mean}	<0.001		<0.001	<0.001
Gray-level cooccurrence matrix (GLCM)	Contrast	<0.001		0.001	<0.001
	Correlation	0.005		0.004	0.007
	Dissimilarity	<0.001		0.001	<0.001
	Homogeneity	<0.001		0.001	<0.001
	Entropy	0.004		0.002	0.015
Gray-level run length matrix (GLRLM)	SRE	<0.001		0.002	<0.001
	LRE	<0.001		0.002	<0.001
	GLNUr	<0.001		<0.001	<0.001
	RP	<0.001		0.001	<0.001
	RLNU	<0.001		<0.001	<0.001
	SRHGE	0.01			0.005
	LRLGE	0.002		0.013	0.001
	LRHGE	0.006		0.009	0.004
Neighborhood gray-level different matrix (NGLDM)	Coarseness	<0.001		<0.001	<0.001
	Contrast	<0.001		<0.001	<0.001
	Busyness	<0.001		<0.001	<0.001
	Complexity	<0.001		<0.001	<0.001
	Strength	<0.001		<0.001	<0.001
Gray-level zone length matrix (GLSZM)	LZE	<0.001		<0.001	<0.001
	GLNUz	0.008			0.003
	ZP	<0.001		0.001	<0.001
	LZLGE	<0.001		<0.001	<0.001
	LZHGE	<0.001		<0.001	<0.001

Abbreviations are the same as those for Table 2.

Note: For each feature in the clinical examination, conventional PET-related parameter, and textural analysis, the overall differences among the FIGO stage I, II, and III–IVA groups were verified using the Kruskal–Wallis test. The overall difference is defined as significance if $P < 0.05$. For the feature with significant differences among FIGO groups, the Mann–Whitney U test was used to examine the differences between any two groups. According to Bonferroni correction, the difference between two subgroups was significant if $P < 0.017$.

that the homogeneity is a reliable parameter for predicting PLN metastasis. It would be interesting that an increased homogeneity value within tumors is linked to higher risk of PLN metastasis. Pearson's correlation coefficient analysis revealed that homogeneity is not correlated with the SUV_{max} (P = 0.45), but it is highly correlated with the MTV and TLG_{mean}

Table 5. Predictive textural indices in differentiating histological types and the area under the ROC curve

Classification of matrix	Index	AUC	*P* value
Tumor marker	SCC-Ag	0.85 ± 0.03	<0.001
	CEA	0.42 ± 0.06	0.176
Conventional PET-related parameter	SUV_{max}	0.56 ± 0.06	0.296
	MTV	0.57 ± 0.06	0.226
	TLG_{mean}	0.59 ± 0.06	0.11
Gray-level cooccurrence matrix (GLCM)	None		
Gray-level run length matrix (GLRLM)	None		
Neighborhood gray-level different matrix (NGLDM)	None		
Gray-level zone length matrix (GLSZM)	SZE	0.37 ± 0.06	0.025
	ZLNU	0.39 ± 0.05	0.05

Abbreviations are the same as those for Table 2.

($P < 0.0001$, R = 0.57 and $P < 0.0001$, R = 0.56, respectively). Therefore, we assumed that an increased tumor burden is directly associated with an elevated LN metastasis risk. Appendix 3 shows that tumors with either a large MTV and high homogeneity or a high TLG_{mean} and homogeneity increased the risk of PLN metastasis. MTVs were presumed to be a key factor affecting the homogeneity because they were also used for calculating the TLG_{mean}. Notably, the homogeneity should be meticulously measured because the MTV would be overestimated if the MTVs are associated with the bladder. Because the uterus is cylindrical with a bottleneck, the cavity within the uterus may simultaneously increase the MTV and homogeneity. This is a plausible reason for the positive correlation between the two factors. Contrastingly, the TLG_{mean} ($MTV \times SUV_{mean}$) may invalidate this assumption. In case of a cavity within the uterus, a decreased SUV_{mean} would lead to a reduced TLG_{mean}. Altogether, this suggests that the calculation of the homogeneity is highly dependent on the extracted MTV, regardless of the existence of cavities.

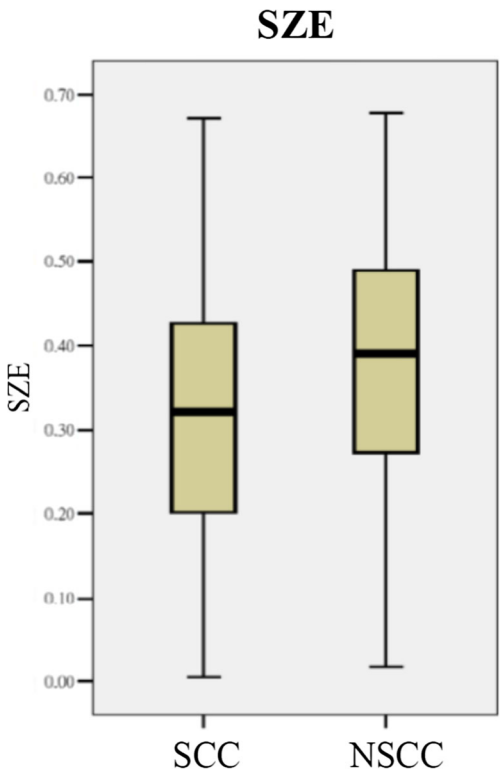

Fig. 4 Quantitative differences in the values of indices between squamous cell carcinoma (SCC; n = 138) and nonsquamous cell carcinoma (NSCC; n = 32)

Tixer et al. [4] conducted a textural study investigating the useful indices for predicting responses to chemoradiotherapy in esophageal cancer; local homogeneity and entropy yielded the most favorable results in the GLCM features to differentiate the treatment responses. In their study, increased homogeneity values were associated with poor responders. Altogether, the biological mechanisms underlying the homogeneity must be examined in future studies, in which treatment outcomes are a study endpoint. In addition, correlation studies between gene expression profiling and the homogeneity index are required.

Although most cervical cancers are related to a latent infection of human papilloma virus, studies have suggested significant changes in the differential expression between SCC and NSCC [31, 32]. To date, few studies have reported the imaging diversities caused by different pathological types. This study is the first to evidence the differences in SZE values between SCC and NSCC, probably because of the disparities in tissue type and density. Although a quantitative association was observed, the molecular mechanisms underlying the change in textural features between the two factors must be investigated. Future studies should integrate gene expression profiling into textural analysis to elucidate the essential biological implications for SZE in tumor tissue engineering. In addition, sequential dynamic changes of SZE after treatment might play a role in determining the outcome and should be more extensively studied.

The findings of this study should be interpreted cautiously because they represent a retrospective study design in a single institute. External validation studies that use a multi-institutional data set with imaging studies and a range of scanners, resolution settings, and reconstruction algorithms are necessary to confirm our findings. Conducting such studies is crucial because textural features can highly depend on reconstruction schemes and imaging parameters. In this setting, disparities between the performance of different PET scanners will become evident and must be discussed. In addition, regardless of the higher accuracy when visualizing the retroperitoneal LN through FDG PET, a correlation study using pathological specimens of patients with cervical cancer receiving PLN or PALN sampling is required to confirm the actual predictive role of imaging analysis. Furthermore, the use of a fixed threshold at 50% of SUVmax to define MTV can potentially lead to underestimation of functional volumes especially in cases of high heterogeneity of intratumoral uptake [33]. Although we found this approach could reduce the probability for the connection between the extracted MTV and the bladder, it will be imperative to compare the superiority and weakness between our method and advanced segmentation algorithms using a contour-based or clustered-based approach for different biological endpoints [30]. Finally, integrating gene expression profiling into the current texture analysis would be more explanatory because it would reveal the molecular pathway underlying intratumoral heterogeneity.

Conclusion

The findings of this study suggest that in patients with cervical cancer, PLN or PALN metastasis can be predicted by using textural feature of homogeneity derived from the GLCM and $TLG_{mean,}$ respectively. In addition, SZE from the GLSZM was the sole textural index associated with quantitative differences between SCC and NSCC. Additional external validation studies are required to confirm these findings.

Acknowledgements This study was supported in part by the Taiwan Ministry of Health and Welfare Clinical Trial and Research Center of Excellence (MOHW106-TDU-B-212-113004); China Medical University Hospital, Academia Sinica Taiwan Biobank Stroke Biosignature Project (BM10501010037); NRPB Stroke Clinical Trial Consortium (MOST105-2325-B-039-003); Tseng-Lien Lin Foundation (Taichung, Taiwan); Taiwan Brain Disease Foundation (Taipei, Taiwan); Katsuzo and Kiyo Aoshima Memorial Funds, Japan; Taiwan Ministry of Science and Technology (MOST 105-2218-E-009-034); and Asia University, Taichung, Taiwan (ASIA-105-CMUH-14); and Welfare Surcharge of Tobacco Products, China Medical University Hospital Cancer Research Center of Excellence (MOHW105-TDU-B-212-134-003, Taiwan). The funders played no role in the study design, data collection and analysis, publication decision, or manuscript drafting. No additional external funding was received for this study.

Author contributions WC Shen, SW Chen, and CH Kao were responsible for design of the study. All authors collected the data. SW Chen, WC Shen, and CH Kao carried out statistical analysis, interpretation of data, and drafting the article. All authors provided some intellectual content. SW Chen, WC Shen, and CH Kao approved the version to be submitted. All authors read and approved the final manuscript. SW Chen and WC Shen are equally contributory to this article.

Compliance with ethical standards

Conflict of interest All authors declare no conflicts of interest.

Ethical approval This study was approved by a local institutional review board DMR99-IRB-010(CR6).

Informed consent The institutional review board specifically waived the consent requirement.

References

1. Hanahan D, Weinberg RA. Hallmarks of cancer: the next generation. Cell. 2011;144:646–74.
2. Asselin MC, O'Connor JP, Boellaard R, Thacker NA, Jackson A. Quantifying heterogeneity in human tumors using MRI and PET. Eur J Cancer. 2012;48:447–55.
3. Chicklore S, Goh V, Siddique M, Roy A, Marsden PK, Cook GJ. Quantifying tumor heterogeneity in 18 F-FDG PET/CT imaging by texture analysis. Eur J Nucl Med Mol Imaging. 2013;40:133–40.
4. Tixier F, Le Rest CC, Hatt M, et al. Intratumor heterogeneity characterized by textural features on baseline 18F-FDG PET images predicts response to concomitant radiochemotherapy in esophageal cancer. J Nucl Med. 2011;52:369–78.
5. Vaidya M, Creach KM, Frye J, Dehdashti F, Bradley JD, El Naqa I. Combined PET/CT image characteristics for radiotherapy tumor response in lung cancer. Radiother Oncol. 2012;102:239–45.
6. Cook GJR, Yip C, Siddique M, et al. Are pretreatment 18F-FDG PET tumor textural features in non-small cell lung cancer associated with response and survival after chemoradiotherapy? J Nucl Med. 2013;54:19–26.
7. Hatt M, Majdoub M, Vallieres M, et al. 18F-FDG PET uptake characterization through texture analysis: investigating the complementary nature of heterogeneity and functional tumor volume in a multi-cancer site patient cohort. J Nucl Med. 2015;56:38–44.
8. Ohri N, Duan F, Snyder BS, et al. Pretreatment 18FDG-PET textural features in locally advanced non-small cell lung cancer: secondary analysis of ACRIN 6668/RTOG 0235. J Nucl Med. 2016.
9. Kidd EA, Grigsby PW. Intratumoral metabolic heterogeneity of cervical cancer. Clin Cancer Res. 2008;14:5236–524.
10. Yang F, Thomas MA, Dehdashti F, Grigsby PW. Temporal analysis of intratumoral metabolic heterogeneity characterized by textural features in cervical cancer. Eur J Nucl Med Mol Imaging. 2013;40:716–27.
11. Ho KC, Fang YH, Chung HW, et al. A preliminary investigation into textural features of intratumoral metabolic heterogeneity in FDG PET for overall survival prognosis in patients with bulky cervical cancer treated with definitive concurrent chemoradiotherapy. Am J Nucl Med Mol Imaging. 2016;6:166–75.
12. Cheng NM, Fang YH, Lee LY, et al. Zone-size nonuniformity of 18F-FDG PET regional textural features predicts survival in patients with oropharyngeal cancer. Eur J Nucl Med Mol Imaging. 2015;42:419–28.

13. Orlhac F, Soussan M, Maisonobe JA, Garcia CA, Vanderlinden B, Buvat I. Tumor texture analysis in 18F-FDG PET: relationships between texture parameters, histogram indices, standardized uptake values, metabolic volumes, and total lesion glycolysis. J Nucl Med. 2014;55:414–22.
14. Stehman FB, Bundy BN, DiSaia PJ, Keys HM, Larson JE, Fowler WC. Carcinoma of the cervix treated with radiation therapy. I. A multi-variate analysis of prognostic variables in the gynecologic oncology group. Cancer. 1991;67:2776–85.
15. Kidd EA, Siegel BA, Dehdashti F, et al. Lymph node staging by positron emission tomography in cervical cancer: relationship to prognosis. J Clin Oncol. 2010;28:2108–13.
16. Yen TC, Ng KK, Ma SY, et al. Value of dual-phase 2-fluoro-2-deoxy-d-glucose positron emission tomography in cervical cancer. J Clin Oncol. 2003;21:3651–8.
17. Reinhardt MJ, Ehritt-Braun C, Vogelgesang, et al. Metastatic lymph nodes in patients with cervical cancer: detection with MR imaging and FDG PET. Radiology. 2001;218:776–82.
18. Chen SW, Hsieh TC, Yen KY, Liang JA, Kao CH. Pretreatment 18F-FDG PET/CT in whole body total lesion glycolysis to predict survival in patients with pharyngeal cancer treated with definitive radiotherapy. Clin Nucl Med. 2014;39:e296–300.
19. Meyer F. Topographic distance and watershed lines. Signal Processing. 1994;38:113–25.
20. Haralick RM, Shanmugam K, Dinstein I. Textural features for image classification. IEEE Trans Syst Man Cybern. 1973;3:610–21.
21. Sun C, Wee WG. Neighboring gray level dependence matrix for texture classification. Comput Vis Graph Image Process. 1983;23:341–52.
22. Loh H, Leu J, Luo R. The analysis of natural textures using run length features. IEEE Trans Ind Electron. 1988;35:323–8.
23. Thibault G, Fertil B, Navarro C, et al. Texture indexes and gray level size zone matrix: application to cell nuclei classification. Pattern Recognit Inf Process. 2009;140–145.
24. Brooks FJ, Grigsby PW. FDG uptake heterogeneity in FIGO IIb cervical carcinoma does not predict pelvic lymph node involvement. Radiat Oncol. 2013;23(8):294.
25. van Velden FH, Kramer GM, Frings V, Nissen IA, Mulder ER, de Langen AJ, Hoekstra OS, Smit EF, Boellaard R. Repeatability of Radiomic Features in Non-Small-Cell Lung Cancer [(18)F]FDG-PET/CT Studies: Impact of Reconstruction and Delineation. Mol Imaging Biol. 2016;18:788–95.
26. Leijenaar RT, Nalbantov G, Carvalho S, van Elmpt WJ, Troost EG, Boellaard R, Aerts HJ, Gillies RJ, Lambin P. The effect of SUV discretization in quantitative FDG-PET Radiomics: the need for standardized methodology in tumor texture analysis. Sci Rep. 2015;5:11075.
27. Desseroit MC, Tixier F, Weber WA, Siegel BA, Cheze Le Rest C, Visvikis D, Hatt M. Reliability of PET/CT shape and heterogeneity features in functional and morphological components of Non-Small Cell Lung Cancer tumors: a repeatability analysis in a prospective multi-center cohort. J Nucl Med. 2016; doi:10.2967/jnumed.116.180919.
28. Tixier F, Hatt M, Le Rest CC, Le Pogam A, Corcos L, Visvikis D. Reproducibility of tumor uptake heterogeneity characterization through textural feature analysis in ^{18}F-FDG PET. J Nucl Med. 2012;53:693–700.
29. Leijenaar RT, Carvalho S, Velazquez ER, van Elmpt WJ, Parmar C, Hoekstra OS, Hoekstra CJ, Boellaard R, Dekker AL, Gillies RJ, Aerts HJ, Lambin P. Stability of FDG-PET Radiomics features: an integrated analysis of test-retest and inter-observer variability. Acta Oncol. 2013;52:1391–7.
30. Hatt M, Tixier F, Pierce L, Kinahan PE, Le Rest CC, Visvikis D. Characterization of PET/CT images using texture analysis: the past, the present… any future? Eur J Nucl Med Mol Imaging. 2017;44:151–65.
31. Contag SA, Gostout BS, Clayton AC, Dixon MH, McGovern RM, Calhoun ES. Comparison of gene expression in squamous cell carcinoma and adenocarcinoma of the uterine cervix. Gynecol Oncol. 2004;95:610–7.
32. Fujimoto T, Nishikawa A, Iwasaki M, Akutagawa N, Teramoto M, Kudo R. Gene expression profiling in two morphologically different uterine cervical carcinoma cell lines derived from a single donor using a human cancer cDNA array. Gynecol Oncol. 2004;93:446–53.
33. Hatt M, Lee J, Schmidtlein CR, El Naqa I, Caldwell C, De Bernardi E, et al. Classification and evaluation strategies of auto-segmentation approaches for PET: Report of AAPM Task Group No. 211. Med Phys. 2017 Jan 24; doi:10.1002/mp.12124.